

Time-resolved transconductance spectroscopy on self-assembled quantum dots: Spectral evolution from single- into many-particle states

A. Beckel,^{1,*} A. Ludwig,² A. D. Wieck,² A. Lorke,¹ and M. Geller¹

¹*Fakultät für Physik and CENIDE, Universität Duisburg-Essen, Lotharstraße 1, Duisburg 47048, Germany*

²*Lehrstuhl für Angewandte Festkörperphysik, Fakultät für Physik und Astronomie, Ruhr-Universität Bochum, Universitätsstraße 150, Bochum 44780, Germany*

(Received 14 March 2014; revised manuscript received 15 April 2014; published 28 April 2014)

Using transconductance spectroscopy we study the tunneling dynamics of electrons from a two-dimensional electron gas (2DEG) into excited and ground states of a layer of self-assembled InAs quantum dots (QDs). From an initially selected nonequilibrium condition, we observe the charging dynamics of the QD states and their spectral evolution for one- and two-electron configurations. Furthermore, we measure the electron emission from the QD states into the 2DEG for the corresponding evolution of the QD-hydrogen and QD-helium spectra. The comparison with theoretically predicted energies, as well as the evaluation of the dynamics in charging and emission, allows us to separate and identify ground and excited electron configurations in the spectral evolution and discuss in detail the observed maxima in the different spectra.

DOI: [10.1103/PhysRevB.89.155430](https://doi.org/10.1103/PhysRevB.89.155430)

PACS number(s): 73.21.La, 73.40.Gk, 73.63.Kv

I. INTRODUCTION

Quantum dots (QDs) are nanoscale objects with confinement in all three spatial directions that behave like artificial atoms and are therefore perfectly suited for fundamental studies on atomlike quantum states in a solid-state environment [1–3]. One type of semiconductor QD—defined by lithography techniques—is especially applicable to address the atomlike quantum states and electron-electron interaction (like Coulomb blockade and correlation) in all-electrical measurements via source, drain, and gate contacts [4]. The other well-known type of QD—the self-assembled QDs [1–3,5,6]—is harder to access in an all-electrically controlled measurement scheme, as these QDs are smaller and a precise positioning is usually only possible in one direction. Therefore, studies on excited [7] and many-particle states [8,9] and their dynamics were performed mostly in an optical measurement setup, where the electron-hole interaction always has to be taken into account [10–15]. However, from an application point of view, self-assembled QDs offer stronger confinement, allowing operations at a higher temperature range [16], as well as perspectives as building blocks in future quantum computing [11,17] or memory devices [18,19], where an all-electrical control of the charge and spin states is desired.

Here we employ a purely electrical measurement technique—the transconductance spectroscopy (TCS)—on an ensemble of self-assembled QDs, which allows us to prepare and detect the many-particle electron states *without* electron-hole interaction in a time-resolved detection scheme via a two-dimensional electron gas (2DEG) [20]. The nonequilibrium excited states of the first two “QD elements” are prepared (QD-hydrogen and QD-helium configurations) and their spectral evolution from nonequilibrium towards equilibrium is studied as well as their electron emission dynamics after charging the corresponding configuration. From the time evolution of these spectra we can clearly identify ground- and excited-state

configurations and discuss in detail the observed maxima in the spectra.

II. EXPERIMENTAL DETAILS

A. Heterostructure and device

A schematic picture of the semiconductor heterostructure grown by molecular beam epitaxy (MBE) is shown in Fig. 1(a). An AlAs/GaAs superlattice was grown on a GaAs substrate followed by an inverted high electron mobility transistor, including a layer of self-assembled InAs QDs. The active region with embedded QDs and 2DEG of the transistor structure is shown in more detail in Fig. 1(b), including the calculated [21] conduction band offset E_C . The 2DEG is formed at an AlGaAs/GaAs interface, which is located 180 nm below the sample surface. At a temperature of 4.2 K a charge carrier density of $n_{2D} = 7 \times 10^{11} \text{ cm}^{-2}$ with a mobility of $\mu_{2D} = 9 \times 10^3 \text{ cm}^2/\text{Vs}$ can be obtained from magnetotransport measurements at zero gate bias. On top of the 2DEG interface, a layer sequence of 15 nm GaAs, followed by 10-nm $\text{Al}_{0.34}\text{Ga}_{0.66}\text{As}$ and another 5-nm GaAs is forming a tunneling barrier into the QDs. The self-assembled QDs are formed by depositing 1.9 ML of InAs, which results in a density of about $8 \times 10^9 \text{ QD}/\text{cm}^2$.

Using standard optical lithography techniques, the heterostructure has been fabricated into transistors as shown in Fig. 1(c). A channel mesa has been defined by etching and Ohmic source-drain contacts were produced by evaporation and subsequent annealing of Ni/AuGe/Au contacts. The source-drain channel was covered with a Schottky gate electrode by evaporation of Ti/Au.

B. Time-resolved transconductance measurement

The transconductance measurements were carried out in a liquid helium bath cryostat at 4.2 K. The electrical connections to the device are shown in Fig. 1(c). The conductance G of the 2DEG is measured with a source contact of the transistor connected to ground and a constant drain voltage of $V_{SD} = 10 \text{ mV}$ is provided by a current amplifier. The amplifier output

*andreas.beckel@uni-due.de

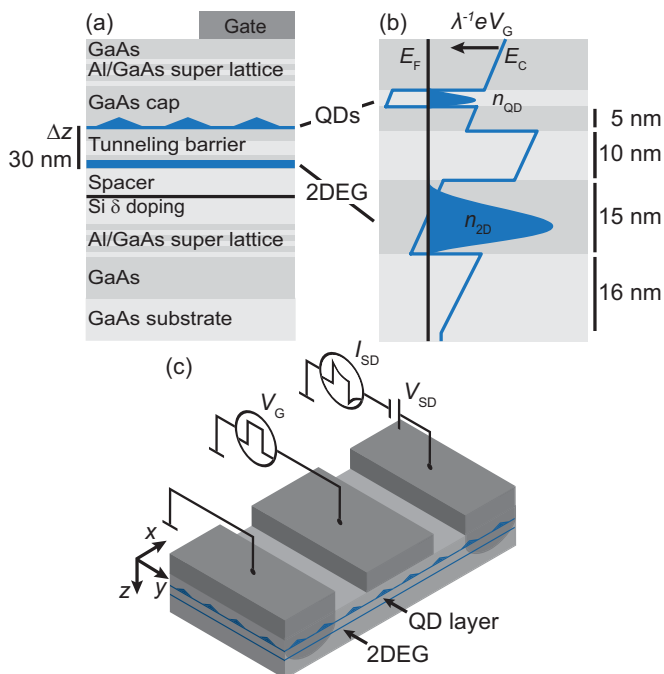


FIG. 1. (Color online) (a) Schematic picture of the heterostructure grown by MBE. (b) Calculated conduction band diagram of the active region with the layer of QDs and the 2DEG. (c) Fabricated transistor structure with source, drain, and gate contacts. The transconductance of the 2DEG is measured via source-drain current I_{SD} as a function of the gate voltage V_G .

is proportional to the source-drain current $I_{SD}(t)$ and measured with a sampling rate of 250 kHz. The measurement is triggered by a function generator which is used to set the gate voltage V_G with respect to the source contact.

The measurements operation principle is shown in Fig. 2. The gate pulse sequence starts in Fig. 2(a) with a gate voltage

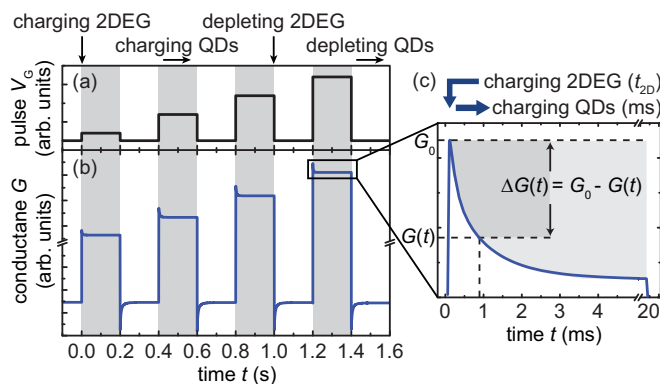


FIG. 2. (Color online) (a) Gate pulse sequence to set the Fermi level of the 2DEG with respect to the QD energy levels for charging (gray shaded area) and depletion of the QDs (white area). The response of the conductance G of the 2DEG to a charging (depletion) pulse consists of a step for charging (depleting) (rise time of $t_{2D} \approx \mu\text{s}$) and a slower transient ($t_{QD} \approx \text{ms}$), which is due to tunneling of electrons into (out of) the confined QD states. (c) A magnification of the conductance G versus time t , which displays a charging transient for electron tunneling into the QD states.

of $V_G = -1$ V, where the QDs are fully depleted (uncharged) as the Fermi energy E_F of the 2DEG is below the energy levels of the dots. At a time $t = 0$ the function generator switches to a higher charging voltage V_G (indicated by the gray shaded area) and the 2DEG will be charged with electrons, visible in Fig. 2(b) as a fast, steplike increase of the conductance G at $t = 0$ until a maximum G_0 is reached [see also Fig. 2(c) at $t = 0$]. The time constant for charging (depletion) of the 2DEG is given by the RC characteristics of the device and the experimental setup. Here, the response time of the 2DEG is on the order of $t_{2D} \approx 1 \mu\text{s}$, which is significantly faster than the tunneling time (inverse tunneling rate) for electrons into the QD states $t_{QD} \approx 1 \text{ms}$. This difference in time constants allows us to evaluate the charging of the QDs independently from the charging of the 2DEG.

The transients of the QD charging in Fig. 2(c) can be used to evaluate the tunneling dynamics into the dots and the energy levels of the QD states. For this we take the difference of the conductance $\Delta G(t) = G_0 - G(t)$, where G_0 is the conductance just after charging the 2DEG. On one hand, a charged layer of QDs depletes a proportional number of electrons in the 2DEG, given by a relation to the lever arm λ : $\Delta n_{QD} = (1 - 1/\lambda) \Delta n_{2D}$ [22]. On the other hand, the conductance of the 2DEG ΔG_{2D} is determined by its conductivity σ , which is given by the charge carrier density as well as mobility: $G \propto \sigma = en_{2D}\mu$. For a small conductance change (here on the order of $\Delta G/G \lesssim 5\%$) we can approximate

$$\Delta G \propto e \left(n_{2D} \frac{d\mu}{dn_{2D}} + \mu \right) \Delta n_{2D}. \quad (1)$$

Since the overall change in μ, n_{2D}, G is small throughout a typical voltage range for the measurement, we assume a constant prefactor for simplicity [23]. This allows us to use the change in conductance as a direct measure for the change in charge carrier concentration in the QD layer:

$$\Delta G \propto \Delta n_{QD}. \quad (2)$$

When starting from an empty QD ensemble, the transferred electrons Δn_{QD} and thus the conductance change ΔG reflects the average occupation number n of the individual QDs. This conductance change is now shown in Fig. 3 at four different charging times, as the states in the QDs evolve from a still time-dependent, nonequilibrium situation $n(t)$ into a steady equilibrium occupation after about 20 ms $n_{\text{eq}} \approx n$ (20 ms). Accordingly, for any gate voltage V_G the conductance change ΔG increases with time t as more electrons are transferred into the QD states, a process which is determined by the individual tunneling rates (see below). The quantized shell structure is already visible in Fig. 3 as steps in the conductance change versus gate voltage.

III. NONEQUILIBRIUM ELECTRON CHARGING DYNAMICS

From the conductance change in Fig. 3 we can now obtain a quantity that is proportional to the density of states, i.e., the number of QD states dn per energy interval dE . If we take

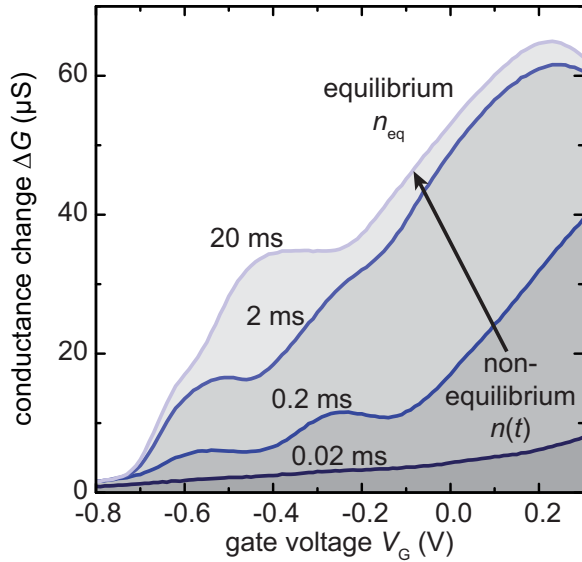


FIG. 3. (Color online) Conductance change $\Delta G \propto \Delta n_{\text{QD}}$ of the 2DEG due to tunneling of electrons into QD states. The equilibrium occupation n_{eq} of the QDs is reached after 20 ms. In equilibrium the QDs are filled with the maximum number of electrons that are possible at this gate voltage V_G .

the first derivative of the conductance change ΔG with respect to the gate voltage V_G , using Eq. (2) and the lever arm λ , we obtain

$$\frac{d\Delta G}{dV_G} = \frac{e}{\lambda} \frac{d\Delta G}{dE} \propto \frac{d\Delta n_{\text{QD}}}{dE} \propto \frac{dn}{dE}. \quad (3)$$

This equation is valid with the assumption made, that the change in conductance ΔG is proportional to the number of electrons Δn_{QD} transferred into the dots, which is again proportional to the electronic states n available for the tunneling process, i.e., the tunneling density of states (TDOS).

Figure 4 shows the first derivative of the conductance change $d\Delta G/dV_G$ as a function of the gate voltage V_G and the charging time t , starting right after the switch in gate voltage at $t = 0.02$ ms to an equilibrium at about 10 ms. For simplicity we call this quantity “time dependent” TDOS in the following.

For a short time after the pulse at $t < 0.1$ ms, the initially empty QDs will, on average, be charged with less than a single electron; i.e., a subensemble is charged with a single electron. The spectrum in Fig. 4, hence, reflects the single-particle spectrum with the one-electron ground state (an electron in the s -shell) at $V_G = -0.66$ V (position 1) and the one-electron excited states (an electron in the p - or d -shell) with maxima at $V_G = -0.35$ V (position 3) and $V_G = 0$ V, respectively. This reflects the excitation spectrum of a QD-hydrogen configuration, which has been discussed in more detail previously [20]. For times larger than the tunneling times (here after approximately 10 ms), the system has reached a steady state and the spectrum evolved into the energy spectrum of many-particle ground states for an ensemble of QDs charged with one to six electrons, filling the s - and p -shells.

By setting the initial gate voltage to $V_0 = -0.62$ V, 90% of the QDs in the ensemble are charged with one electron in the

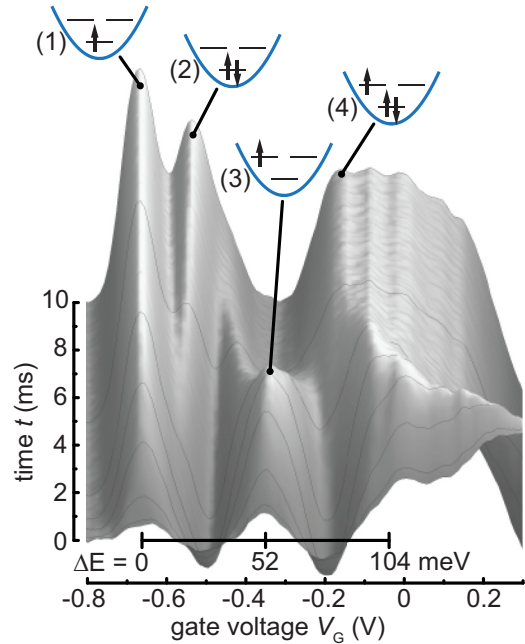


FIG. 4. (Color online) The density of states (TDOS) as a function of gate voltage V_G and time t . The QDs are initially empty and for short times after the pulse, the TDOS reflects the single-particle spectrum, where maximum (3) is related to the single-electron configuration in the p -shell, located 52 meV above the single-electron ground state in the s -shell (1). The spectrum evolves into the equilibrium spectrum at $t = 10$ ms, where the two-electron and three-electron ground states are visible as maxima at positions (2) and (4), respectively.

s -shell. The resulting spectrum shown in Fig. 5 is now sensitive to the two-electron spectrum of a QD-helium configuration at short times and evolves again into the steady-state configuration after about $t = 10$ ms. The ground state of the QD-helium spectrum here determines our reference energy $\Delta E = 0$ meV, where the two electrons occupy the s -shell with antiparallel spins, i.e., a spin-singlet state. The first excited state is a spin-triplet state with two parallel spins and an additional energy of $\Delta E = 42$ meV relative to the ground state. The second excited state at $\Delta E = 52$ meV (see Ref. [20] for reference) is a spin-singlet state; however, it is not yet clearly distinguishable from the rising three-electron ground state (3) in Fig. 5. In Sec. IV we separate these states and discuss them in more detail.

A. Time evolution of the density of states

From the time-dependent TDOS of the QD-hydrogen and QD-helium configuration, shown in Figs. 4 and 5, respectively, we now want to discuss the transition from the nonequilibrium into the equilibrium situation, which is determined by the respective rates of the sequential charging processes. In the following we show how to distinguish excited states from (many-particle) ground states within the time evolution of the spectra.

Figure 6(a) shows cross sections of the spectrum in Fig. 4 along the time axis at voltages labeled with (1) to (4), while Fig. 6(b) displays schematically the corresponding charging

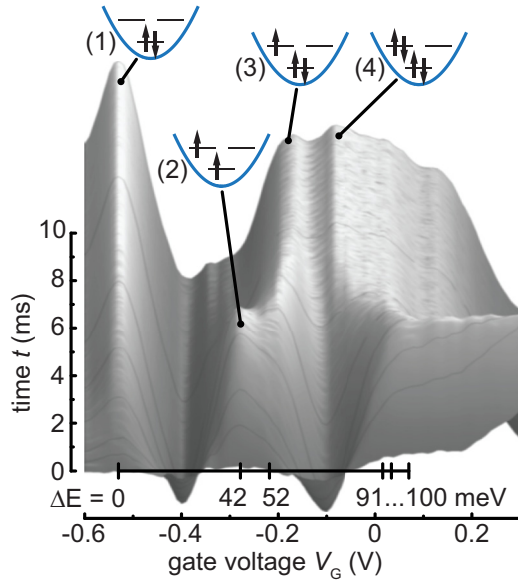


FIG. 5. (Color online) The time evolution of the density of states for a QD ensemble initially filled with one electron before applying the charging pulse V_G . The displayed two-particle energies for short times reflects the nonequilibrium excited two-electron states. Clearly visible is a two-electron triplet state at 42 meV [maximum (2)], while the two-electron singlet state at 52 meV cannot be separated from the rising three-electron ground state [maximum (3)].

sequence. Note that in the broadened ensemble, the average occupation number n is given by the probability p_n to find a QD at a given occupation by $n = \sum n p_n$. Here we start from completely empty QDs ($n = 0$); i.e., all QDs are in the initial condition $p_0 = 1$. At voltage position (1), 50% of the ensemble will be charged with a single electron after the transition time of 10 ms into equilibrium, i.e., $p_1 = 0.5$, and the transition from nonequilibrium to equilibrium at this voltage position reads $p_0 = 1 \rightarrow 0.5$ and $p_1 = 0 \rightarrow 0.5$. The time scale for the transition into equilibrium is given by the charging time of the first electron at voltage position (1), which we can determine to $\tau_1 = 1/\gamma_1 \approx 1.4$ ms from the transient (1) shown in Fig. 6(a).

For $V_G = -0.52$ V [position (2) in Fig. 4], the composition of the ensemble in equilibrium after the transition time is given by $p_1 = 0.5, p_2 = 0.5$; i.e., half of the QDs in the ensemble will be charged with one electron and half with two electrons, respectively. Here we obtain a peculiarly long time constant of $\tau_1 + \tau_2 \approx 5$ ms $> 2\tau_1$, which we attribute to a delay from charging the first electron, as the Fermi energy is initially aligned between the empty s - and p -shells [see Fig. 6(b)].

Turning to the first excited energy of the hydrogen configuration, we find a steep increase in tunneling rate, reducing the time constant for adding the first electron to 0.5 ms as indicated in sequence (3) of Fig. 6(b). This causes a peak in the spectrum of Fig. 4 at $V_G = -0.35$ V. After a relaxation process from the p -shell, the equilibrium condition of the transient at $t = 20$ ms requires all QDs to be charged with two electrons, completely filling the s -shell leading to $dn_{\text{eq}}/dV_G = 0$. In the corresponding evolution (3) in Fig. 6(a) we also observe a decreasing amplitude after about 1 ms.

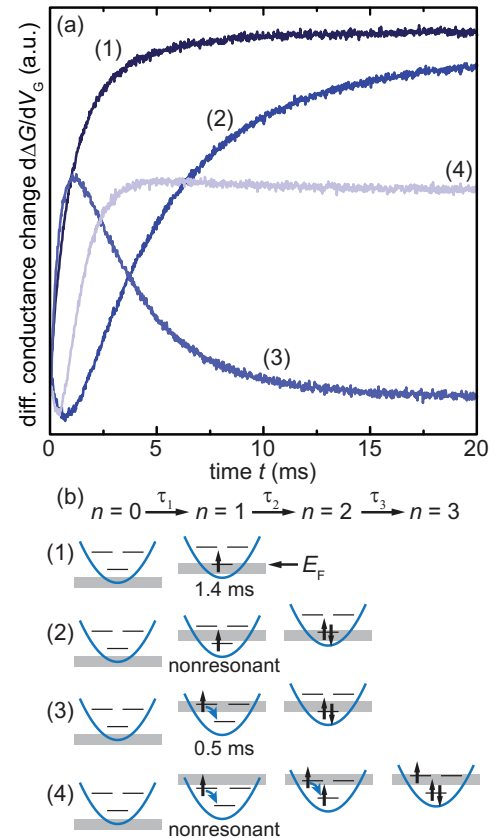


FIG. 6. (Color online) (a) Cross sections of Fig. 4 along the indicated voltages. (b) Corresponding charging sequence for an average QD from empty ($n = 0$) to equilibrium occupation. The evolution is governed by the sequential time constants τ_n . Processes (1) and (3) correspond to resonant charging of the first electron, when the Fermi energy is aligned with the single-particle levels. For processes (2) and (4) the charging rate decreases (negative slope at the beginning) since no QD levels are aligned to the Fermi edge. The excited peak (3) vanishes due to the rise of the ground state (2).

The equilibrium condition $dn_{\text{eq}}/dV_G = 0$ is reached after two electrons have been transferred, so the time-constant of the decrease is determined by filling the two electrons at position (2). Accordingly, we derive the characteristic behavior of an excited state as a faster rise time compared to the ground state followed by a decrease into equilibrium. For process (4) we again observe a fast rise ($\tau_3 \approx 0.7$ ms), comparable to the time we found for the first electron of sequence (3) also charging via the p -shell. As for sequence (2), we again observe a delay, because the Fermi energy is initially aligned in between the p - and the d -shell.

Sequences (2) and (4) also show a small negative signal at early times. Here the states in the 2DEG are aligned in between two shells of the empty QDs. The tunneling process for the first electron becomes nonresonant and its rate γ_1 decreases. For short times t , the average occupation is given by $n \approx \gamma_1 t$. Since we take the derivative with respect to the gate voltage [cf. Eq. (3)], the spectrum becomes negative as γ_1 decreases with increasing gate voltage. Although tunneling at positions (2) and (4) are initially nonresonant in both cases, process (4) still appears faster compared to (2). Since the gate voltage

at position (4) is higher, the tunneling barrier is effectively reduced for those electrons tunneling at the Fermi energy, which increases the tunneling rate even in this nonresonant condition.

From the evaluation of the charging transients in Fig. 6 we can now sort the maxima obtained in Fig. 4 for the nonequilibrium situation just after the gate pulse into ground and excited QD states. The amplitude of an excited state will rise fast and then decay again, if no ground state is overlapping at the same voltage (i.e., no peak in the equilibrium spectrum exists); a situation which is fulfilled for charging the excited p -state, represented by the transient of sequence (3). However, the situation is more complicated if ground states overlap in energy for the final (steady-state) configuration with the excited nonequilibrium states, a situation which is present for the excited state of the d -shell at $V_G = 0$ V. Using the emission spectroscopy in Sec. IV enables us also to clearly separate ground and excited states for such a situation.

We want to discuss now the time evolution of different cross sections of the second spectrum, where initially the QDs are filled with one electron, the so-called QD-helium [20], and its time evolution into equilibrium. The cross sections for the spectrum of Fig. 5 (prepared with

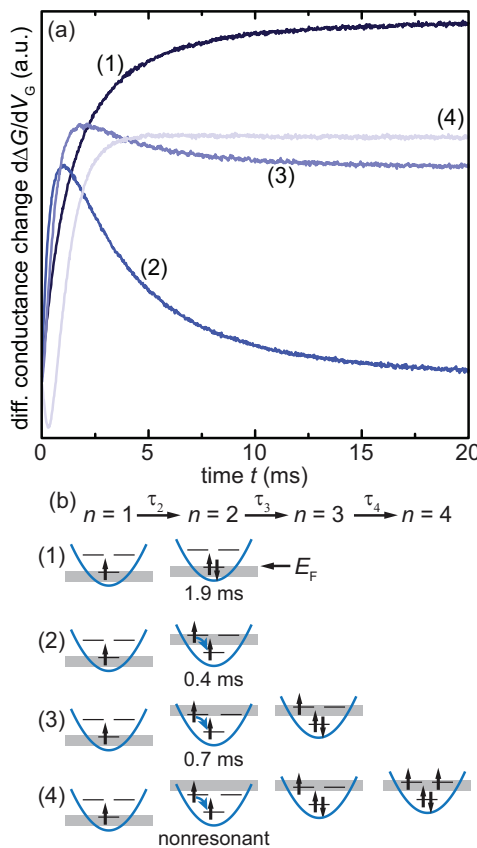


FIG. 7. (Color online) Time evolution (a) of initially charged QDs (Fig. 5) for the charging sequences in (b). The two-electron spectrum is shifted towards higher energy, which allows a fast filling of (3) compared to Fig. 6, sequence (4). For sequence (4) a negative slope at the beginning is caused by tunneling below the Fermi energy for the two-electron configuration.

a single charge) are shown in Fig. 7. From sequence (1) we can determine the charging time $\tau_2 \approx 2$ ms for the two-electron ground-state configuration. In sequence (2), the second electron is charged from the p -shell and we find a decrease of the amplitude after a maximum at about $t \approx 1$ ms, a clear signature for an excited-state configuration of the electron, here the spin triplet configuration, as assigned before [20].

In sequence (3), the spectral distribution of the lower-energy dots which are still charged from the p -shell and the higher-energy dots which are charged off-resonantly between p - and d -shell are mixed. Although the equilibrium density does not vanish at voltage (3) compared to (2) an overshoot can be observed around $t = 2$ ms, caused by the overlap of nonequilibrium and equilibrium peaks. This indicates that a maximum in the transient is, as mentioned before, not a sufficient requirement for identifying nonequilibrium (excited) states. At sequence (4) the majority of the ensemble is charged off resonance and the time scales of the charging sequence are comparable to Fig. 6, sequence (4).

Evaluating the evolution of the charging processes makes it possible to derive information about the individual rates in the sequential process, but is also disadvantageous when many-particle and single-particle voltages are strongly overlapping as for the single-electron d -shell and the many-particle p -shell electrons. This limitation can be overcome due to the difference in tunneling barrier for the emission process when the QD ensemble gets depleted, as shown in the next section.

IV. EMISSION SPECTROSCOPY

In the previous sections, the change in conductance during the charging of the QDs and its evolution in time have been investigated. Instead of measuring the response upon switching to the charging voltage V_G , it is also possible to evaluate the conductance change after switching back to the depletion voltage V_0 (see Fig. 8) and evaluate the emission of electrons instead.

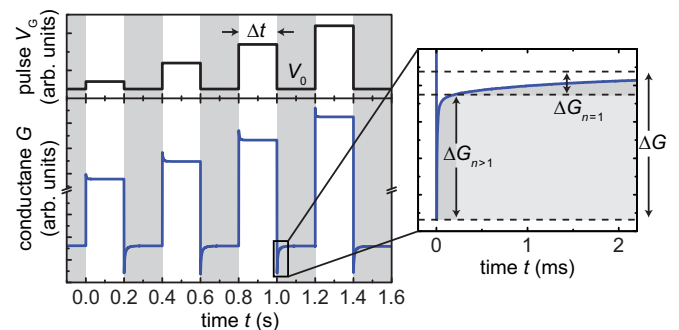


FIG. 8. (Color online) Measurement cycle for the emission spectroscopy. The conductance change ΔG during emission after a charging time Δt is separated into fast $\Delta G_{n>1}$ and slow $\Delta G_{n=1}$ processes. The fast emission results from QDs occupied with more than one electron, i.e., $n > 1$, while the slow emission originates from the emission of the last electron, i.e., $n = 1$. To obtain the spectra shown in Fig. 9(b), the charging time Δt was fixed to 0.1 ms.

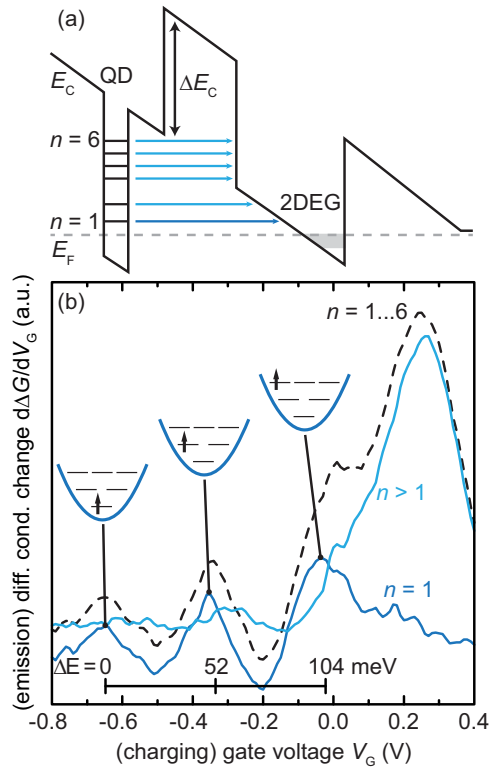


FIG. 9. (Color online) (a) Energy diagram for a pulse, completely depleting a QD after charging six electrons and (b) emission spectrum after a 0.1-ms charging pulse V_G . Tunneling probability increases exponentially with the occupation number n , which makes it possible to separate the full emission spectrum (dashed line) into fast ($t < 0.2$ ms) processes for configurations with $n > 1$ electrons and slow processes ($t > 0.2$ ms), corresponding to the single-particle spectrum with $n = 1$.

For this, we prepare a spectrum by interrupting the charging process after a certain time Δt , e.g., 0.1 or 1 ms. The relaxation of excited states into the ground states during the charging process is fast compared to the tunneling and can be considered instantaneous. Thus, when switching to the depletion voltage, all QDs can already be considered in the ground-state configuration. Figure 9(a) then shows the conduction band E_C for the emission process right after switching to the depletion voltage. Here the depicted QD is still charged with six electrons. As the ground-state energies of the QD are elevated with the number of electrons n , the tunneling rate for the higher states increases over orders of magnitude due to their decreasing conduction band offset ΔE_C . This difference in time scales allows us to separate the QDs, charged with a certain number of electrons n .

For the QD-hydrogen spectrum, the slowest emission is obtained for an occupation $n = 1$ with a characteristic time constant of $\tau_1 \approx 2$ ms. We see in Fig. 9(a) that the ground state with $n = 1$ has the highest tunneling barrier. Electrons from higher occupations $n \geq 2$, on the other hand, are almost completely emitted within the first 0.2 ms. This allows us to separate the overall conductance change $\Delta G \propto n_{\text{eq}}$ of the emission process into a part $\Delta G_{n=1} = G$ (50 ms) – G (0.2 ms), which is only sensitive to the single-electron

configurations with $n = 1$, by only measuring these slow processes [25]. The remaining part $\Delta G_{n>1} = G$ (0.2 ms) – G_0 then contains all the fast processes, where the dots have already been charged with more than a single electron $n > 1$.

In Fig. 9(b) the derivative d/dV_G of the two separated contributions are shown after a charging pulse of 0.1 ms for the hydrogen configuration. The dashed line shows the full emission spectrum after 50 ms, which corresponds to the charging spectrum in Fig. 4 after 0.1 ms. The separation revealing the single-particle spectrum for $n = 1$, consisting of the three peaks corresponding to increased charging rate from resonant tunneling into the s -, p -, and d -shells. In each case, the single electron relaxes into the ground state and tunnels out on the slow time scale. The charging process becomes significantly faster as V_G is increased and parts of the ensemble for $V_G > 0$ V are already charged with more than one electron ($n > 1$) even after a short pulse of 0.1 ms. The QDs with higher occupation are emitting considerably faster and only contribute to the spectrum shown as the line labeled $n > 1$ in Fig. 9.

Filtering the spectrum with respect to occupation becomes more important when the overlap of the single-particle and equilibrium spectrum becomes stronger, obscuring the initial resonances as observed in Fig. 5.

Figure 10(a) shows the separated contributions for the ensemble initially charged with one electron after a charging pulse of 1 ms. Here the depletion voltage was increased to leave a residual electron, so the slowest emission process is from the occupation $n = 2$. In the charging spectrum in Fig. 5, the inhomogeneously broadened peaks from charging the second and third electrons via the p -shell are overlapping at $V_G = -0.25$ V. The emission measurement, however, allows us to separate the nonequilibrium resonances from the equilibrium spectrum for charging pulses even at these intermediate times. The black dashed line represents again the overall charging spectrum for all electron occupations $n = 2, \dots, 6$. The overlapping resonance can now clearly be separated into two different electron configurations: (i) the two-electron triplet state with a calculated energy separation of 42 meV, seen for slow emission processes in the line labeled $n = 2$, and (ii) the three-electron ground state, seen for faster emission processes in the line labeled $n > 2$. The two-electron singlet state at an expected separation of 52 meV cannot be clearly resolved, but may very well contribute as a shoulder to the dominant triplet maximum at approximately $V_G = -0.2$ V. Since we observe only the *change* in tunneling rate $d\gamma_2/dV_G$ at early times, we can explain the dominant triplet by a stronger increase of the tunneling rate, if we increase the gate voltage to $V_G = -0.3$ V (charging the triplet) than for $V_G = -0.2$ V (charging the singlet). The stronger increase in tunneling rate leads to a higher amplitude of the differential conductance change in Fig. 10. We can give two possible reasons for this effect. (i) For the triplet, we increase the gate voltage from a nonresonant situation (reduced tunneling probability) to a resonant situation (enhanced tunneling probability) by charging the p -shell, while we have a comparable tunneling probability for the singlet, as tunneling occurs always resonantly into the p -shell. Hence, the change in tunneling rate is less significant for the singlet and the amplitude of this state at $V_G = -0.2$ V

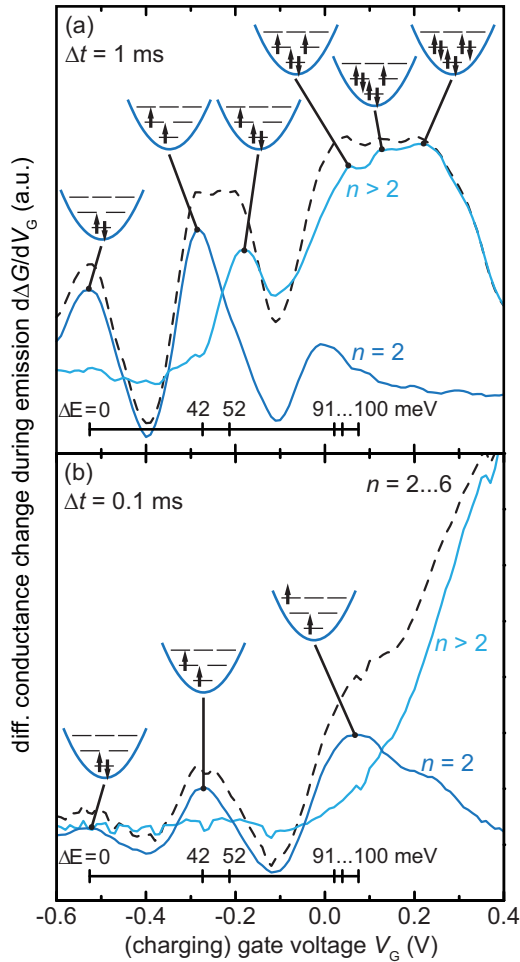


FIG. 10. (Color online) Emission spectra after a charging pulse of (a) 1 ms and (b) 0.1 ms, depleting the dots to one residual electron. Separating the full emission spectrum (dashed line) into fast and slow processes makes it possible to separate the $n = 2$ excitation spectrum from the configurations with $n > 2$. The separation still reveals the nonequilibrium spectrum even for an intermediate charging time of 1 ms, but attenuating the peak from the d -shell, which is clearly identifiable after charging for only 0.1 ms.

in Fig. 10 is reduced. (ii) The triplet has a three times higher degeneracy than the singlet excited state [20]; hence, a higher tunneling probability and a stronger change in tunneling rate versus gate voltage.

Another maximum which can be assigned to the d -shell is clearly visible in the $n = 2$ line at about $V_G = 0$ V; however, in contrast to the peak from the p -shell it appears attenuated, which is an effect of the long charging time. At the higher gate voltages, most of the QDs in the ensemble have already been charged with two electrons after 1 ms so there is no change in emission with respect to gate voltage and the derivative for $n = 2$ is quenched. After a charging time of 0.1 ms the average occupation is smaller than $n = 2$ even at the higher gate voltages. Figure 10(b) shows the corresponding emission spectrum, where we can clearly identify the position of the maximum for $n = 2$ resulting from tunneling into the d -shell. Again, we only observe one significant maximum at a separation of 100 meV while the calculation predicts a

TABLE I. Comparison of energy separations from calculated [20] hydrogen or helium (triplet) states vs experiment.

	ΔE_{s-p} (meV)	ΔE_{s-d} (meV)
	Hydrogen	
Experiment	50	103
Theory	52	104
	Helium	
Experiment	43	100
Theory	42	94

series of closely packed energy levels. Here the width of the ensemble may limit the resolution. For comparison we use the state with an energy separation of 94 meV (fourth state in Fig. 4 of Ref. [20]). This state has a dominant contribution from the s -state in the single-particle basis, which is the initial condition for our experiment with one electron in the s -shell [26].

Table I compares the obtained energy separations from the emission spectra of QD-hydrogen and QD-helium to the calculated energies of Ref. [20]. For QD-helium we only compare to the triplet configurations, since we assume they contribute foremost to the tunneling rate. Although the measurement is sensitive to an energy-dependent tunneling rate, we find the average energy values obtained from the experiment are in good agreement with the predicted values for the hydrogen and helium configurations.

V. CONCLUSION

In summary, we have analyzed the electronic excitation spectra for the QD elements hydrogen and helium. During the charging process, the density of states evolves from a preselected nonequilibrium (either hydrogen or helium) with its respective excited states into the many-particle ground states. Compared to the ground states, the spectral evolution of an excited state shows a faster increasing amplitude in the beginning, followed by a decrease into the equilibrium condition. For a high density of overlapping many-particle states, we can additionally use the emission spectroscopy to filter only the pure elemental contributions in the spectrum from hydrogen or helium. This allows us to clearly identify the respective shell structures up to the d -shell for both elements, in good agreement with the calculated energies.

ACKNOWLEDGMENTS

The authors would like to thank Benjamin Baxevanis and Daniela Pfannkuche for fruitful discussions. This work was supported by the DFG (Contract No. GE 2141/1-1) in the framework of NanoSci-E+ Project No. QD2D of the European Commission and the Mercator Research Center Ruhr (MERCUR) of Stiftung Mercator, as well as Project No. QuaHL-Rep 16BQ1035 and ‘‘Hochfunktionale Speicher’’ (HOFUS) within the VIP program of the BMBF.

- [1] S. Tarucha, D. G. Austing, T. Honda, R. J. van der Hage, and L. P. Kouwenhoven, *Phys. Rev. Lett.* **77**, 3613 (1996).
- [2] S. Tarucha, D. G. Austing, Y. Tokura, W. G. van der Wiel, and L. P. Kouwenhoven, *Phys. Rev. Lett.* **84**, 2485 (2000).
- [3] T. Fujisawa, D. G. Austing, Y. Tokura, Y. Hirayama, and S. Tarucha, *Nature (London)* **419**, 278 (2002).
- [4] S. Lindemann, T. Ihn, T. Heinzel, W. Zwerger, K. Ensslin, K. Maranowski, and A. C. Gossard, *Phys. Rev. B* **66**, 195314 (2002).
- [5] D. Bimberg, N. Kirstaedter, N. N. Ledentsov, Zh. I. Alferov, P. S. Kop'ev, and V. M. Ustinov, *IEEE J. Sel. Top. Quantum Electron.* **3**, 196 (1997).
- [6] P. M. Petroff, A. Lorke, and A. Imamoglu, *Phys. Today* **54**, 46 (2001).
- [7] P. Hawrylak, G. A. Narvaez, M. Bayer, and A. Forchel, *Phys. Rev. Lett.* **85**, 389 (2000).
- [8] G. Jundt, L. Robledo, A. Hoge, S. Falt, and A. Imamoglu, *Phys. Rev. Lett.* **100**, 177401 (2008).
- [9] T. Köppen, D. Franz, A. Schramm, C. Heyn, D. Heitmann, and T. Kipp, *Phys. Rev. Lett.* **103**, 037402 (2009).
- [10] A. Zrenner, E. Beham, S. Stuffer, F. Findeis, M. Bichler, and G. Abstreiter, *Nature (London)* **418**, 612 (2002).
- [11] M. Kroutvar, Y. Ducommun, D. Heiss, M. Bichler, D. Schuh, G. Abstreiter, and J. J. Finley, *Nature (London)* **432**, 81 (2004).
- [12] A. Högele, S. Seidl, M. Kroner, K. Karrai, R. J. Warburton, B. D. Gerardot, and P. M. Petroff, *Phys. Rev. Lett.* **93**, 217401 (2004).
- [13] M. Ediger, G. Bester, A. Badolato, P. M. Petroff, K. Karrai, A. Zunger, and R. J. Warburton, *Nat. Phys.* **3**, 774 (2007).
- [14] N. A. J. M. Kleemans, J. van Bree, A. O. Govorov, J. G. Keizer, G. J. Hamhuis, R. Notzel, A. Y. Silov, and P. M. Koenraad, *Nat. Phys.* **6**, 534 (2010).
- [15] A. V. Kuhlmann, J. Houel, A. Ludwig, L. Greuter, D. Reuter, A. D. Wieck, M. Poggio, and R. J. Warburton, *Nat. Phys.* **9**, 570 (2013).
- [16] T. Nowozin, A. Marent, G. Hönig, A. Schliwa, D. Bimberg, A. Beckel, B. Marquardt, A. Lorke, and M. Geller, *Phys. Rev. B* **84**, 075309 (2011).
- [17] T. D. Ladd, F. Jelezko, R. Laflamme, Y. Nakamura, C. Monroe, and J. L. O'Brien, *Nature (London)* **464**, 45 (2010).
- [18] M. Geller, C. Kapteyn, L. Müller-Kirsch, R. Heitz, and D. Bimberg, *Phys. Status Solidi B* **238**, 258 (2003).
- [19] A. Marent, M. Geller, A. Schliwa, D. Feise, K. Pötschke, D. Bimberg, N. Akçay, and N. Öncan, *Appl. Phys. Lett.* **91**, 242109 (2007).
- [20] B. Marquardt, M. Geller, B. Baxevanis, D. Pfannkuche, A. D. Wieck, D. Reuter, and A. Lorke, *Nat. Commun.* **2**, 209 (2011).
- [21] G. L. Snider, 1d poisson/schrödinger: A band diagram calculator, <http://www3.nd.edu/~gsnider>, University of Notre Dame, Notre Dame, IN.
- [22] M. Ruß, C. Meier, A. Lorke, D. Reuter, and A. D. Wieck, *Phys. Rev. B* **73**, 115334 (2006).
- [23] For more details on the individual contributions, see Ref. [24].
- [24] B. Marquardt, A. Beckel, A. Lorke, A. D. Wieck, D. Reuter, and M. Geller, *Appl. Phys. Lett.* **99**, 223510 (2011).
- [25] The time of 0.2 ms to separate the fast and slow processes was determined from the emission spectrum after fully charging the QDs, showing the equilibrium (ground-state) spectrum in the overall conductance change $d\Delta G/dV_G$, as seen in Fig. 4 for long times. We then used the spectrum for the slow processes and increased this separation time until the maxima from ground states with $n > 1$ are suppressed, leaving only the one-electron ground state in the spectrum.
- [26] The other calculated states from Ref. [20] may also be available for tunneling, but would require an additional change in quantum number of the prepared electron before tunneling can occur (i.e., higher-order tunneling).